Mechanistic Insights into Photochemical Reactions on CH3NH3PbBr3 Perovskite Nanoparticles from Single-Particle Photoluminescence Spectroscopy

Kimura, Yuki

Karimata, Izuru

Kobori, Yasuhiro

Tachikawa, Takashi

(Citation)
ChemNanoMat,5(3):340-345

(Issue Date)
2019-03

(Resource Type)
journal article

(Version)
Accepted Manuscript

Mechanistic Insights into Photochemical Reactions on $CH_3NH_3PbBr_3$ Perovskite Nanoparticles from Single-Particle Photoluminescence Spectroscopy

Yuki Kimura,[a] Izuru Karimata,[a] Yasuhiro Kobori, [a, b] and Takashi Tachikawa* [a, b]

Abstract: Metal halide perovskites have attracted considerable attention in applications such as photovoltaic cells and light-emitting diodes. The performance and durability of perovskite devices are significantly dependent on the nature of structural defects, but the underlying mechanisms of structure-related photochemical reactions are not yet fully elucidated. This study demonstrates that the photoluminescence (PL) from individual perovskite nanoparticles (NPs) can be utilized to resolve the different trapping pathways of the photogenerated charges, and hence, obtain a correlation between the pathways. PL deactivation and activation were observed and mainly attributed to nonradiative Auger recombination by the trapped charges and the passivation of surface traps by oxygen, respectively. Single-particle spectroelectrochemical technique was further employed to explore the possible origin of the effective charge trap states and the reversibility of redox events under electrical bias. Consequently, this study unravels the complex effects of the structural defects on the charge carrier dynamics in perovskites.

Introduction

Organic lead halide perovskites $MAPbX_3$ (MA = $CH_3NH_3^+$, X = Cl^-, Br^-, or I^-), composed of methyl ammonium, lead, and halide ions (Figure 1a), have attracted considerable attention for photovoltaic applications[1] and light-emitting devices[2] owing to their strong light absorption,[3] high photoluminescence (PL) quantum yield,[4] long charge carrier diffusion lengths,[5] band-like charge carrier transport,[6] and photon recycling ability.[7] Structural disorders or defects strongly affect these properties, often leading to serious problems in the aforementioned applications. One such effect is the anomalous hysteresis or poor reproducibility in the current density–voltage (*J*–*V*) characteristics of the perovskite solar cells.[8] There is considerable debate about its origin, and arguments include charge trapping/detrapping, ion migration, and ferroelectric switching.[9] A recent study suggests that the hysteresis behavior is due to the formation of iodide Frenkel defects caused by the accumulation of excess electrons at iodide vacancy (V_I) sites (i.e., $V_I^\bullet + 2e^- \rightarrow V_I'$ in Kröger–Vink notation), rather than the migration of the vacancy.[10] Subsequently, the long-term durability of the perovskite layer remains a concern because of the intrinsic structural instability of the perovskite in ambient air.[11] Moreover, the degradation of the perovskite layer is significantly driven by external factors such as heat,[12] light,[13] moisture,[14] oxygen,[15] and electrical bias.[16]

Since several types of defects play crucial roles in most of these behaviors, and a further mechanistic understanding of the defect-related carrier dynamics is necessary for improving the performance and durability of the perovskite devices. However, due to the inherent heterogeneities in the sample and the accumulation of diffusing charge carriers at the interfaces between the different domains in a polycrystal or closely packed nanoparticles (NPs),[17] cooperative or non-cooperative responses of the charge carriers to a few traps cannot be readily resolved by conventional bulk measurements only. In this respect, isolated perovskite nanostructures that are not in contact with others are preferable. For instance, our group reported a significant intermittency and stepwise enhancement of PL from single $MAPbBr_3$ NPs because of charge trapping by only a few effective trap sites.[18]

In this study, perovskite NPs were synthesized and the PL of individual particles was observed by several single-particle microscopy techniques. The $MAPbBr_3$ was selected because of its better stability against moisture as compared with $MAPbI_3$.[19] For the cases where the PL intensity changed by more than one order of magnitude during photoexcitation, the PL deactivation and activation were found to be linked mainly to the nonradiative Auger recombination by trapped charges and the passivation of surface traps by oxygen, respectively. Furthermore, single-particle spectroelectrochemistry measurements were performed to explore the redox events and their reversibility in the individual perovskite NPs under applied bias potential. Our single-particle study reveals the complex effects of the trap sites on the charge carrier dynamics in the perovskites.

Results and Discussion

Figure 1b shows the optical absorption and PL spectra of $MAPbBr_3$ NPs in diethyl ether. The absorption band is broad and has an edge at around 530 nm. In the PL spectrum, an emission maximum was seen at around 530 nm, which is typical of the PL of $MAPbBr_3$ NPs.[18] From the transmission electron microscopy images, it was confirmed that the synthesized $MAPbBr_3$ NPs had a mean diameter of about 10 to several tens of nanometers.[18]

[a] Y. Kimura, I. Karimata, Prof. Y. Kobori, Prof. T. Tachikawa
Department of Chemistry, Graduate School of Science
Kobe University
1–1 Rokkodai–cho, Nada–ku, Kobe 657–8501, Japan
E-mail: tachikawa@port.kobe-u.ac.jp
[b] Prof. Y. Kobori, Prof. T. Tachikawa
Molecular Photoscience Research Center
Kobe University
1–1 Rokkodai–cho, Nada–ku, Kobe 657–8501, Japan

Supporting information for this article is given via a link at the end of the document.

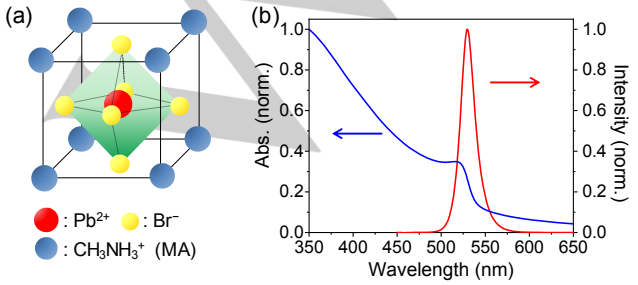

Figure 1. (a) Structure of $MAPbBr_3$. (b) Optical absorption (blue) and PL (red) spectra of $MAPbBr_3$ NPs in diethyl ether. The excitation wavelength for PL measurement was 405 nm

To investigate the PL properties of the individual $MAPbBr_3$ NPs, a colloidal solution of $MAPbBr_3$ was spin-coated on the cover glass, and single-particle measurements were performed using space- and time-resolved fluorescence microscope. Figure 2 depicts the typical single-particle PL of $MAPbBr_3$ observed during 405-nm laser irradiation in ambient air. Figures 2a and b show that the PL intensity from each NP is strong immediately after light irradiation, but weakens significantly within a few seconds (referred to as PL deactivation). In addition to the decrease in the PL intensity, the PL decay lifetimes were considerably shortened without any noticeable spectral peak shift (Figures 2c and d). After continuous excitation for a few of tens of seconds, the NPs start emitting again and regain their initial intensity (referred to as PL activation). This gradual increase indicates the light-induced passivation of the nonradiative intrinsic defects, known as photoactivation or photocuring.[20] After the activation process has been completed, the PL intensity remains constant, suggesting that atmospheric moisture does not cause significant degradation of the samples. PL activation is also accompanied by the gradual increase of the average lifetime ($<\tau>$) of the PL decay (Figure 2e). Moreover, a small blue shift (3 nm) with respect to the initial state, before PL deactivation, was observed during PL activation (blue and red spectra, Figure 2c). In a previous study, a gradual blue shift of the PL peak during the illumination of single CdSe quantum dots in air was ascribed to photooxidation of the surface.[21]

These processes have been focused here to elucidate the mechanism of the photochemical reactions. For the characterization of PL deactivation, t_d was defined as time until the PL intensity decays to the minimum level and was analyzed by single-exponential curve fitting for each particle (blue line in Figure 2b). In the case of PL activation, the corresponding t_a was determined by the exponential growth fits of the early data points obtained after PL deactivation (red line in Figure 2b).[22] This is because it takes long time to reach the maximum under weak excitation conditions.

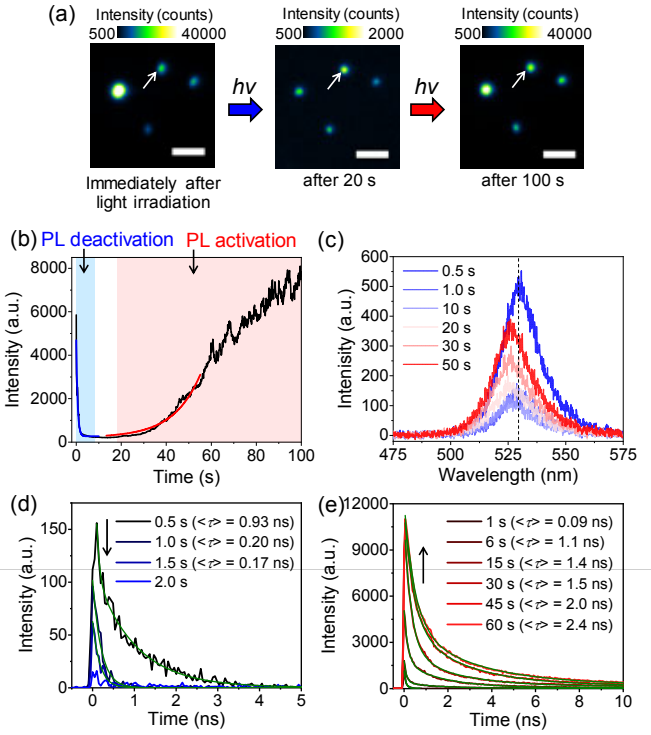

Figure 2. (a) Single-particle PL images of $MAPbBr_3$ NPs observed during 405-nm laser irradiation in ambient air. The scale bars are 2 μm. (b) The PL intensity trajectory of the particle indicated by an arrow in panel (a). The blue and red lines are the fitted curves (analytical procedures of characteristic times (t_d and t_a) are given in the main text). (c) Temporal changes of the PL spectra. Normalized PL decay profiles observed for different particles during PL deactivation (d) and activation (e). The decay profiles in (d) and (e) were fitted by a single or double exponential function (green lines). The average lifetimes ($<\tau>$) are given in the figure legend. No reliable lifetime could be obtained for the profile at 2 s in panel (d) due to its low intensity.

To investigate the effect of light irradiation on t_d and t_a, their dependence on the excitation intensity in ambient air was examined first. It is evident from Figures 3a and b that both PL deactivation and activation are light-induced processes. The wide range of t_d and t_a values indicate the heterogeneous nature of the sample. The t_d values decrease sharply while the t_a values decrease gradually with increasing excitation intensity. The absence of any clear correlation between t_d and t_a, as seen from the single-particle analysis, suggests that the two processes obey different mechanisms (Figure 3c).

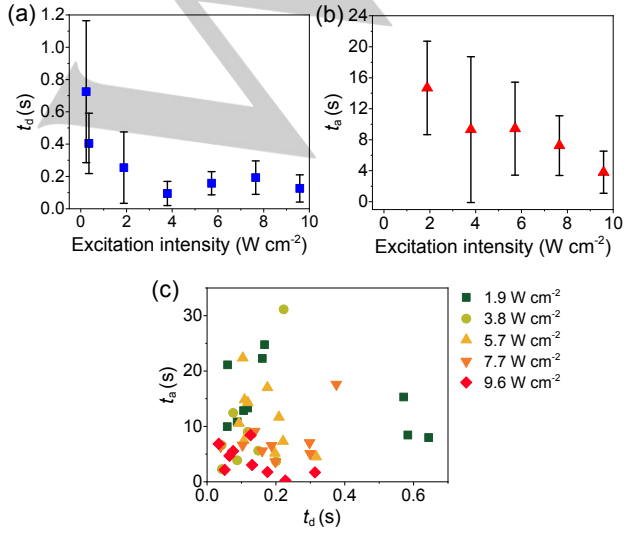

Figure 3. Dependences of t_d (a) and t_a (b) on the excitation intensity at the cover glass surface. At least eight particles were analyzed for each excitation intensity. (c) Correlation between t_d and t_a. The total number of analyzed particles is 47.

Here, the possible mechanisms proposed for each process are discussed and are illustrated in Figure 4. There are two proposed mechanisms for PL deactivation. In the first mechanism, light irradiation produces a number of new defects that result in PL quenching through charge trapping, eventually leading to the degradation of the perovskite structure (Figure 4a).[23] The other mechanism is based on the Auger recombination in which an electron-hole pair recombines nonradiatively by transferring its energy to a trapped charge (Figure 4b).[17c] This trap-assisted Auger recombination is remarkably enhanced by decreasing size of NPs.[24]

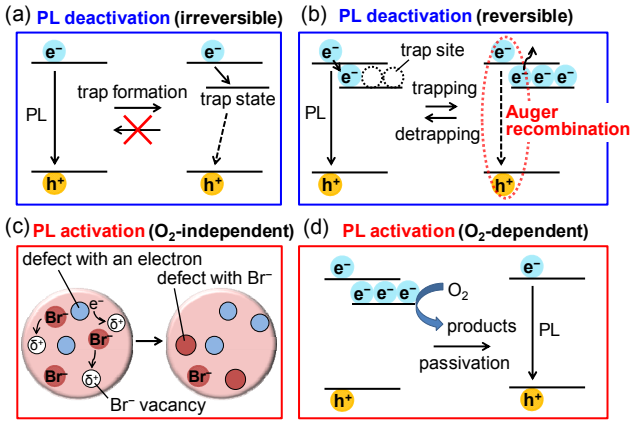

Figure 4. Possible mechanisms of PL deactivation (a, b) and activation (c, d). The broken arrows indicate the nonradiative charge recombination.

Next, the two possible mechanisms for PL activation are discussed. In the first mechanism, the photogenerated electrons are trapped at the intrinsic bromide ion vacancies (V_{Br}), and this reaction promotes the vacancy-interstitial recombination by electrostatic repulsion between trapped electrons (i.e., V_{Br}') and diffusing bromide ions (Figure 4c). This mechanism successfully explained the gradient in the activated region in the $MAPbI_3$ perovskite films.[25] In the second mechanism, the effective trap sites such as the halide ion vacancies, halide ion interstitials, and lead interstitials are deactivated by the interaction or reaction with molecular oxygen under light irradiation (Figure 4d).[20a, 26]

The mechanisms of PL deactivation/activation were clarified by the reversibility tests. When light irradiation was stopped before PL activation could occur, PL deactivation was repeated several times despite slight differences in the t_d values among the cycles (Figure 5a). If light irradiation produces permanent defects in NPs, such repeatability is not expected because the degradation is usually irreversible.[23] Gottesman et al. reported that the structural transformation led to a slow reversible PL deactivation that required several hours for recovery in the dark.[27] This time scale is far more than those in the phenomena observed in this study. Therefore, it is suggested that the PL deactivation in the present system is caused by the Auger recombination (Figure 4b) rather than mechanism of Figure 4a. As shown in Figure 2, the NPs have very low PL yields and short lifetimes during the PL deactivation in their dim states until their neutrality is restored, or the trap states disappear. On the other hand, when light irradiation was paused during the PL activation and then restarted, the PL intensity continued to increase, without any PL deactivation (Figure 5b). This continuity suggests that PL activation originates form the irreversible structural changes in NPs, and its mechanism is totally different from the reversible deactivation mechanism.

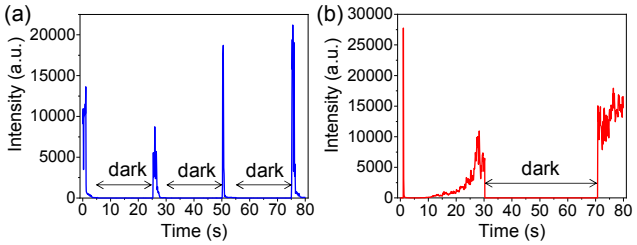

Figure 5. (a) The repeatability of PL deactivation in air. (b) The continuity of PL activation in air.

Very recently, Hong et al. reported similar PL behavior in $MAPbI_3$ microcrystals in the time scale of a few to tens of seconds.[28] They proposed that interstitial iodide (I_i) and lead (Pb_i) defects are responsible for the PL activation and deactivation, respectively. However, the kind of reactions involved in these processes are still unclear. To gain more information on PL activation, the effect of oxygen molecules on this process was examined.

Figure 6a demonstrates that the PL from single NPs quickly weakened in Ar atmosphere, similar to that observed in air, but there was no activation even after prolonged exposure to intense laser radiation. However, a gradual increase in the PL intensity was clearly observed immediately after the sample was exposed to air, thereby indicating the necessity of gaseous oxygen for activation. The photogeneration of carriers, in the absence of oxygen, is known to increase the densities of both halide vacancies in the crystalline structure and neutral iodine in the interstitial sites. This occurs due to the enhanced ion conductivity within the perovskite, thereby leading to a more defective lattice.[29] This concept, however, cannot explain the current observation wherein the PL intensity increases again upon combined exposure to light and air (Figure 6). It is thus suggested that the trap sites disappear by surface reaction with oxygen molecules, leading to the PL activation, and this is not directly correlated with PL deactivation (Figure 3c), possibly due to the different locations of the relevant defects. In line with this observation, Anaya et al. reported that simultaneous exposure of $MAPbBr_3$ films to light and gaseous oxygen resulted in the formation of superoxide species.[22] The density functional theory (DFT) calculations further predicted that the adsorbed molecular oxygen captures an electron to form superoxide species capable of passivating surface V_I.[30] This mechanism was also in good agreement with the claim in a previous report from our group.[18] Another possibility was put forward by Meggiolaro et al., who, using hybrid DFT calculations including spin-orbit coupling, suggested that oxygen effectively inactivates deep hole traps associated with I_i in $MAPbI_3$ by forming moderately stable oxidized products (i.e., IO^-, IO_2^-, and IO_3^-).[31]

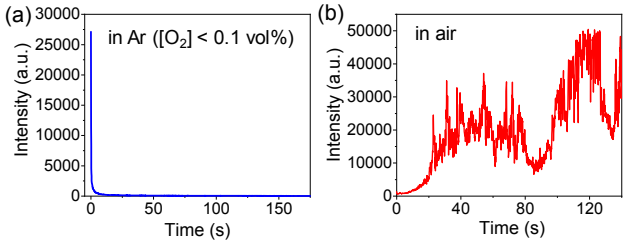

Figure 6. PL intensity trajectories of the same NP observed (a) in Ar ($[O_2] \leq$ 0.1 vol%) and (b) after exposing to air. After the PL deactivation, air was introduced into the sample chamber.

Finally, single-particle spectroelectrochemical measurements were carried out under a microscope with an electrochemical analyzer in a standard three-electrode setup to characterize the nature of the effective traps (Figure 7a). The indium tin oxide (ITO)-coated cover glass was employed as the working electrode, Pt was employed as the counter electrode, and Ag wire in dichloromethane containing 0.1 M Bu_4NPF_6 was used as a pseudo-reference electrode. The NPs were immobilized on the ITO surface, possibly via electrostatic interactions. When negative bias was applied using cyclic voltammetry (−0.05 V → −0.95 V → −0.05 V vs normal hydrogen electrode (NHE)), the PL intensity sharply decreased at around −0.9 V vs NHE, followed by the recovery in intensity at a less negative voltage (Figure 7b). A similar PL response was observed for other NPs (Figure S1). The potentials at which quenching and recovery of the PL occur are different among the particles and are −0.85 ± 0.06 and −0.42 ± 0.17 V vs NHE for the two processes, respectively. The observed PL quenching is reasonably explained by assuming that the electrochemically-injected electrons in the trap state that are close to the bottom of the conduction band (CB) (−0.84 V vs NHE for bulk $MAPbBr_3$)[32] quench the excitons via Auger recombination. It is believed that this state is related to the PL deactivation and possibly originates from V_{Br}, which is also supported by DFT calculations.[33] The mechanism of PL recovery is still obscure, but is usually ascribed to the disappearance of excess electrons.

In contrast, when positive bias was applied (0.06 V → 1.26 V → 0.06 V vs NHE), the PL intensity sharply decreased at around 0.89 V vs NHE and did not recover at higher voltages (Figures 7c and S1). This was due to the degradation of the perovskite structure by the following oxidation reaction: $CH_3NH_3PbBr_3 - e^- \rightarrow PbBr_2 + CH_3NH_3^+ + 0.5Br_2$.[32b] On the basis of the above results, it is suggested that the photogenerated or electrochemically-injected electrons are captured at the shallow traps, most probably the V_{Br} sites, just at the bottom of the CB. These trapped electrons likely lead to the PL quenching via nonradiative Auger recombination. The irreversible PL quenching occurred at an applied potential of 0.85 ± 0.15 V vs NHE, suggesting that the deeply trapped holes, probably at interstitial ion sites, will induce the degradation of the perovskite structure if not scavenged quickly.

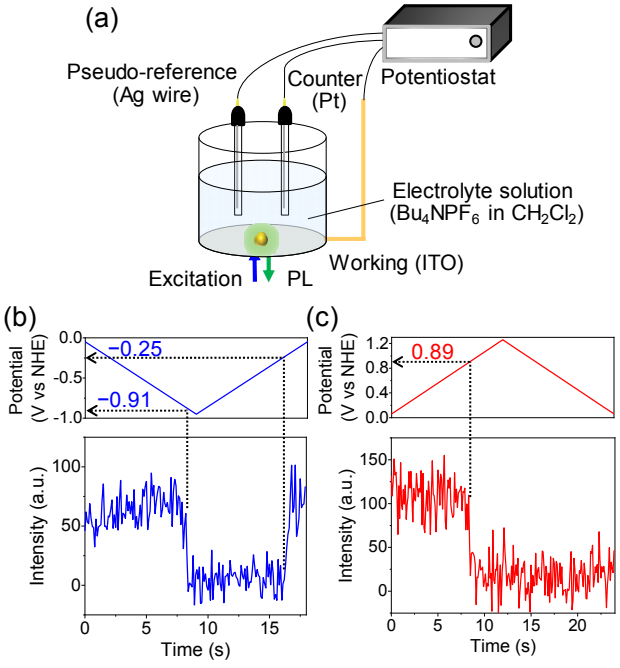

Figure 7. (a) Illustration of the experimental setup for single-particle spectroelectrochemistry. Dependence of the PL intensity on applied (b) negative and (c) positive potential.

Conclusions

In conclusion, significant changes in the PL properties of $MAPbBr_3$ NPs under light irradiation were observed using single-particle PL spectroscopy. The PL deactivation and activation were mainly due to the nonradiative Auger recombination by trapped charges and passivation of surface traps by oxygen in air, respectively. The single-particle spectroelectrochemical studies revealed that the PL from single $MAPbBr_3$ NPs was reversibly quenched by excess electrons in shallow traps near the bottom of the CB, while the perovskite irreversibly degraded under a potential of around 0.9 V vs NHE. Although a direct relationship between the observed activation/deactivation and device instability problems such as the *J–V* hysteresis is still not evident, the findings and methodologies in this study provide further insights into the photo(electro)chemistry of metal halide perovskites.

Experimental Section

Colloidal $MAPbBr_3$ NPs were synthesized without any capping reagents and characterized according to a previous report from our group.[18] In brief, a precursor solution (equimolar concentrations MABr and $PbBr_2$ in *N*,*N*-dimethylformamide) was added to diethyl ether under vigorous stirring. Optical properties of the prepared $MAPbBr_3$ NPs were studied using a UV-visible spectrophotometer (V-770, JASCO) and a fluorescence spectrophotometer (FP-8300, JASCO). The suspensions of NPs were spin-coated on clean borosilicate cover glasses (Matsunami Glass) or ITO-coated cover glasses (Matsunami Glass; 100 nm thickness, 10 Ω cm^{-2} surface resistivity) for observation under the fluorescence microscope. The single-particle PL measurements were performed on a home-built wide-field confocal microscope equipped with a Nikon Ti-E inverted fluorescence microscope.[18, 34] The PL images were recorded using an electron-multiplying charge-coupled device camera (Evolve 512, Roper Scientific) using Micro-Manager (https://www.micro-manager.org/). The 405-nm continuous wave laser (OBIS 405LX, Coherent) or 405-nm pulsed diode laser (PiL040X, Advanced Laser Diode System, 45-ps FWHM) was used to excite the samples. A dichroic mirror (Di02-R405, Semrock) and a longpass filter (BLP01-458R, Semrock) were used to filter the scattering from excitation light. For the spectroscopy, only the emission that passed through a slit entered the imaging spectrograph (MS3504i, SOL instruments) equipped with a CCD camera (DU416A-LDC-DD, Andor). The data were analyzed using ImageJ (http://rsb.info.nih.gov/ij/) and Origin 2018 (OriginLab). For time-resolved PL measurements, the emitted photons were passed through a 100-μm pinhole and then directed onto a single-photon avalanche diode (SPD-050, Micro Photon Devices). The signals from the detector were sent to a time-correlated single photon counting module (SPC-130EM, Becker & Hickl) for further analysis. The instrument response function of the system was around 100 ps. The multiexponential PL decay curves were fitted using a nonlinear least squares method with a double exponential function. The average lifetime $<\tau>$ was then determined using the equation $<\tau> = (a_1\tau_1^2 + a_2\tau_2^2)/(a_1\tau_1 + a_2\tau_2)$, where τ and a are the lifetime and amplitude, respectively. To examine the influence of oxygen, the sample was enclosed in a homemade sample chamber, and the oxygen concentration inside the chamber was adjusted by an Ar gas purge. The oxygen concentration inside the chamber was measured by an oxygen analyzer (maxO2+, Maxtec). The relative humidity was controlled between 40–50% using a dehumidifier. Single-particle electrochemical measurements were carried out using an electrochemical analyzer (model 608E, ALS) with a standard three-electrode configuration.[35] The potentials were determined using the ferrocene/ferrocenium redox couple ($E_{1/2}$ = 0.70 V vs NHE in dichloromethane)[36] as an internal standard and NHE as the reference. All the experiments were conducted at room temperature.

Acknowledgements

This work was partially supported by JSPS KAKENHI Grant Numbers JP15H03771, JP18H01944, JP18H04517, and others.

Keywords: charge transfer • fluorescence imaging • metal halide perovskites • photoluminescence • single-particle spectroscopy

[1] a) A. Kojima, K. Teshima, Y. Shirai, T. Miyasaka, *J. Am. Chem. Soc.* **2009**, *131*, 6050-6051; b) M. M. Lee, J. Teuscher, T. Miyasaka, T. N. Murakami, H. J. Snaith, *Science* **2012**, *338*, 643-647; c) M. A. Green, A. Ho-Baillie, H. J. Snaith, *Nat. Photonics* **2014**, *8*, 506-514.

[2] a) Z.-K. Tan, R. S. Moghaddam, M. L. Lai, P. Docampo, R. Higler, F. Deschler, M. Price, A. Sadhanala, L. M. Pazos, D. Credgington, F. Hanusch, T. Bein, H. J. Snaith, R. H. Friend, *Nat. Nanotechnol.* **2014**, *9*, 687-692; b) G. Xing, N. Mathews, S. S. Lim, N. Yantara, X. Liu, D. Sabba, M. Grätzel, S. Mhaisalkar, T. C. Sum, *Nat. Mater.* **2014**, *13*, 476-480.

[3] S. De Wolf, J. Holovsky, S.-J. Moon, P. Loper, B. Niesen, M. Ledinsky, F.-J. Haug, J.-H. Yum, C. Ballif, *J. Phys. Chem. Lett.* **2014**, *5*, 1035-1039.

[4] a) I. L. Braly, D. W. de Quilettes, L. M. Pazos-Outon, S. Burke, M. E. Ziffer, D. S. Ginger, H. W. Hillhouse, *Nat. Photonics* **2018**, *12*, 355-361; b) N. Droseros, G. Longo, J. C. Brauer, M. Sessolo, H. J. Bolink, N. Banerji, *ACS Energy Lett.* **2018**, *3*, 1458-1466.

[5] a) S. D. Stranks, G. E. Eperon, G. Grancini, C. Menelaou, M. J. P. Alcocer, T. Leijtens, L. M. Herz, A. Petrozza, H. J. Snaith, *Science* **2013**, *342*, 341-344; b) G. Xing, N. Mathews, S. Sun, S. S. Lim, Y. M. Lam, M. Grätzel, S. Mhaisalkar, T. C. Sum, *Science* **2013**, *342*, 344-347.

[6] L. M. Herz, *ACS Energy Lett.* **2017**, *2*, 1539-1548.

[7] L. M. Pazos-Outon, M. Szumilo, R. Lamboll, J. M. Richter, M. Crespo-Quesada, M. Abdi-Jalebi, H. J. Beeson, M. Vrucinic, M. Alsari, H. J. Snaith, B. Ehrler, R. H. Friend, F. Deschler, *Science* **2016**, *351*, 1430-1433.

[8] a) H.-S. Kim, N.-G. Park, *J. Phys. Chem. Lett.* **2014**, *5*, 2927-2934; b) H. J. Snaith, A. Abate, J. M. Ball, G. E. Eperon, T. Leijtens, N. K. Noel, S. D. Stranks, J. T.-W. Wang, K. Wojciechowski, W. Zhang, *J. Phys. Chem. Lett.* **2014**, *5*, 1511-1515.

[9] a) A. Dualeh, T. Moehl, N. Tetreault, J. Teuscher, P. Gao, M. K. Nazeeruddin, M. Gratzel, *ACS Nano* **2014**, *8*, 362-373; b) Y. Shao, Z. Xiao, C. Bi, Y. Yuan, J. Huang, *Nat. Commun.* **2014**, *5*, 5784; c) C. Li, S. Tscheuschner, F. Paulus, P. E. Hopkinson, J. Kiessling, A. Koehler, Y. Vaynzof, S. Huettner, *Adv. Mater.* **2016**, *28*, 2446-2454; d) G. Richardson, S. E. J. O'Kane, R. G. Niemann, T. A. Peltola, J. M. Foster, P. J. Cameron, A. B. Walker, *Energy Environ. Sci.* **2016**, *9*, 1476-1485; e) R. S. Sanchez, V. Gonzalez-Pedro, J.-W. Lee, N.-G. Park, Y. S. Kang, I. Mora-Sero, J. Bisquert, *J. Phys. Chem. Lett.* **2014**, *5*, 2357-2363; f) Y. Kutes, L. Ye, Y. Zhou, S. Pang, B. D. Huey, N. P. Padture, *J. Phys. Chem. Lett.* **2014**, *5*, 3335-3339.

[10] D.-Y. Son, S.-G. Kim, J.-Y. Seo, S.-H. Lee, H. Shin, D. Lee, N.-G. Park, *J. Am. Chem. Soc.* **2018**, *140*, 1358-1364.

[11] a) T. A. Berhe, W.-N. Su, C.-H. Chen, C.-J. Pan, J.-H. Cheng, H.-M. Chen, M.-C. Tsai, L.-Y. Chen, A. A. Dubale, B.-J. Hwang, *Energy*

Environ. Sci. **2016**, *9*, 323-356; b) D. Wang, M. Wright, N. K. Elumalai, A. Uddin, *Sol. Energy Mater. Sol. Cells* **2016**, *147*, 255-275.

[12] a) G. Divitini, S. Cacovich, F. Matteocci, L. Cina, A. Di Carlo, C. Ducati, *Nat. Energy* **2016**, *1*, 15012; b) A. F. Akbulatov, S. Y. Luchkin, L. A. Frolova, N. N. Dremova, K. L. Gerasimov, I. S. Zhidkov, D. V. Anokhin, E. Z. Kurmaev, K. J. Stevenson, P. A. Troshin, *J. Phys. Chem. Lett.* **2017**, *8*, 1211-1218.

[13] a) T. Leijtens, G. E. Eperon, S. Pathak, A. Abate, M. M. Lee, H. J. Snaith, *Nat. Commun.* **2013**, *4*, 3885/3881-3885/3888; b) W. Nie, J.-C. Blancon, A. J. Neukirch, K. Appavoo, H. Tsai, M. Chhowalla, M. A. Alam, M. Y. Sfeir, C. Katan, J. Even, S. Tretiak, J. J. Crochet, G. Gupta, A. D. Mohite, *Nat. Commun.* **2016**, *7*, 11574; c) H. Yuan, E. Debroye, K. Janssen, H. Naiki, C. Steuwe, G. Lu, M. Moris, E. Orgiu, H. Uji-i, F. De Schryver, P. Samori, J. Hofkens, M. Roeffaers, *J. Phys. Chem. Lett.* **2016**, *7*, 561-566.

[14] a) Z. Song, A. Abate, S. C. Watthage, G. K. Liyanage, A. B. Phillips, U. Steiner, M. Grätzel, M. J. Heben, *Adv. Energy Mater.* **2016**, *6*, 1600846. doi: 10.1002/aenm.201600846; b) J. Yang, B. D. Siempelkamp, D. Liu, T. L. Kelly, *ACS Nano* **2015**, *9*, 1955-1963; c) Z. Song, N. Shrestha, S. C. Watthage, G. K. Liyanage, Z. S. Almutawah, R. H. Ahangharnejhad, A. B. Phillips, R. J. Ellingson, M. J. Heben, *J. Phys. Chem. Lett.* **2018**, *9*, 6312-6320; d) G. E. Eperon, S. N. Habisreutinger, T. Leijtens, B. J. Bruijnaers, J. J. van Franeker, D. W. deQuilettes, S. Pathak, R. J. Sutton, G. Grancini, D. S. Ginger, R. A. J. Janssen, A. Petrozza, H. J. Snaith, *ACS Nano* **2015**, *9*, 9380-9393.

[15] a) N. Aristidou, I. Sanchez-Molina, T. Chotchuangchutchaval, M. Brown, L. Martinez, T. Rath, S. A. Haque, *Angew. Chem., Int. Ed.* **2015**, *54*, 8208-8212; b) D. Bryant, N. Aristidou, S. Pont, I. Sanchez-Molina, T. Chotchunangatchaval, S. Wheeler, J. R. Durrant, S. A. Haque, *Energy Environ. Sci.* **2016**, *9*, 1655-1660.

[16] S. Bae, S. Kim, S.-W. Lee, K. J. Cho, S. Park, S. Lee, Y. Kang, H.-S. Lee, D. Kim, *J. Phys. Chem. Lett.* **2016**, *7*, 3091-3096.

[17] a) Y. Tian, A. Merdasa, M. Peter, M. Abdellah, K. Zheng, C. S. Ponseca, T. Pullerits, A. Yartsev, V. Sundstroem, I. G. Scheblykin, *Nano Lett.* **2015**, *15*, 1603-1608; b) A. Merdasa, Y. Tian, R. Camacho, A. Dobrovolsky, E. Debroye, E. L. Unger, J. Hofkens, V. Sundstroem, I. G. Scheblykin, *ACS Nano* **2017**, *11*, 5391-5404; c) X. Wen, A. Ho-Baillie, S. Huang, R. Sheng, S. Chen, H.-c. Ko, M. A. Green, *Nano Lett.* **2015**, *15*, 4644-4649.

[18] T. Tachikawa, I. Karimata, Y. Kobori, *J. Phys. Chem. Lett.* **2015**, *6*, 3195-3201.

[19] J. H. Noh, S. H. Im, J. H. Heo, T. N. Mandal, S. I. Seok, *Nano Lett.* **2013**, *13*, 1764-1769.

[20] a) Y. Tian, M. Peter, E. Unger, M. Abdellah, K. Zheng, T. Pullerits, A. Yartsev, V. Sundstroem, I. G. Scheblykin, *Phys. Chem. Chem. Phys.* **2015**, *17*, 24978-24987; b) E. Mosconi, D. Meggiolaro, H. J. Snaith, S. D. Stranks, F. De Angelis, *Energy Environ. Sci.* **2016**, *9*, 3180-3187; c) Y. Tian, A. Merdasa, E. Unger, M. Abdellah, K. Zheng, S. McKibbin, A. Mikkelsen, T. Pullerits, A. Yartsev, V. Sundstroem, I. G. Scheblykin, *J. Phys. Chem. Lett.* **2015**, *6*, 4171-4177.

[21] S. R. Cordero, P. J. Carson, R. A. Estabrook, G. F. Strouse, S. K. Buratto, *J. Phys. Chem. B* **2000**, *104*, 12137-12142.

[22] M. Anaya, J. F. Galisteo-Lopez, M. E. Calvo, J. P. Espinos, H. Miguez, *J. Phys. Chem. Lett.* **2018**, *9*, 3891-3896.

[23] A. Merdasa, M. Bag, Y. Tian, E. Kaellman, A. Dobrovolsky, I. G. Scheblykin, *J. Phys. Chem. C* **2016**, *120*, 10711-10719.

[24] A. W. Cohn, A. M. Schimpf, C. E. Gunthardt, D. R. Gamelin, *Nano Lett.* **2013**, *13*, 1810-1815.

[25] D. W. de Quilettes, W. Zhang, V. M. Burlakov, D. J. Graham, T. Leijtens, A. Osherov, V. Bulovic, H. J. Snaith, D. S. Ginger, S. D. Stranks, *Nat. Commun.* **2016**, *7*, 11683.

[26] H. Uratani, K. Yamashita, *J. Phys. Chem. Lett.* **2017**, *8*, 742-746.

[27] R. Gottesman, L. Gouda, B. S. Kalanoor, E. Haltzi, S. Tirosh, E. Rosh-Hodesh, Y. Tischler, A. Zaban, C. Quarti, E. Mosconi, F. De Angelis, *J. Phys. Chem. Lett.* **2015**, *6*, 2332-2338.

[28] D. Hong, Y. Zhou, S. Wan, X. Hu, D. Xie, Y. Tian, *ACS Photonics* **2018**, *5*, 2034-2043.

[29] G. Y. Kim, A. Senocrate, T.-Y. Yang, G. Gregori, M. Graetzel, J. Maier, *Nat. Mater.* **2018**, *17*, 445-449.

[30] R. Brenes, C. Eames, V. Bulovic, M. S. Islam, S. D. Stranks, *Adv. Mater. (Weinheim, Ger.)* **2018**, *30*, n/a.

[31] D. Meggiolaro, E. Mosconi, F. De Angelis, *ACS Energy Lett.* **2017**, *2*, 2794-2798.

[32] a) P. Schulz, E. Edri, S. Kirmayer, G. Hodes, D. Cahen, A. Kahn, *Energy Environ. Sci.* **2014**, *7*, 1377-1381; b) G. F. Samu, R. A. Scheidt, P. V. Kamat, C. Janaky, *Chem. Mater.* **2018**, *30*, 561-569.

[33] T. Shi, W.-J. Yin, F. Hong, K. Zhu, Y. Yan, *Appl. Phys. Lett.* **2015**, *106*, 103902/103901-103902/103905.

[34] I. Karimata, Y. Kobori, T. Tachikawa, *J. Phys. Chem. Lett.* **2017**, *8*, 1724-1728.

[35] T. Tachikawa, T. Ochi, Y. Kobori, *ACS Catal.* **2016**, *6*, 2250-2256.

[36] N. G. Connelly, W. E. Geiger, *Chem. Rev.* **1996**, *96*, 877-910.